Electronic supplementary information (ESI)

Cuttlebone-inspired PMIA Membranes with Symmetric Porous Structure for Enhanced Stability of Ultrafiltration

Jiaqing Su[a,b], Yuxiang Zhu[a], Cheng Huang[a,c], Yixin Luo[a,c], Dexin Kong[a], Jingyao Wang[a], Xiao Chen[a,b,c,], and Pengchao Zhang[a,b,c,*]*

a. State Key Laboratory of Advanced Technology for Materials Synthesis and Processing, School of Materials Science and Engineering, Wuhan University of Technology, Wuhan 430070, China.

b. Hubei Longzhong Laboratory, Wuhan University of Technology Xiangyang Demonstration Zone, Xiangyang 441000, China.

c. Sanya Science and Education Innovation Park, Wuhan University of Technology, Sanya 572024, China.

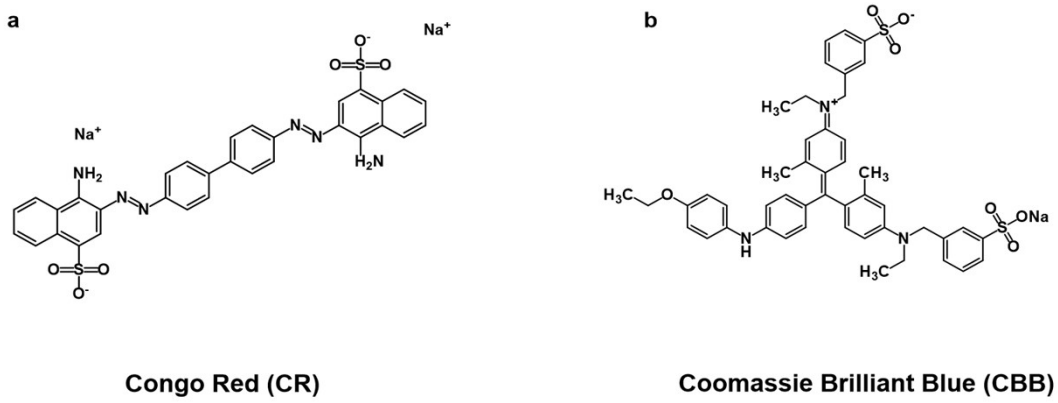

Fig. S1 Chemical structure of (a) Congo Red and (b) Coomassie Brilliant Blue.

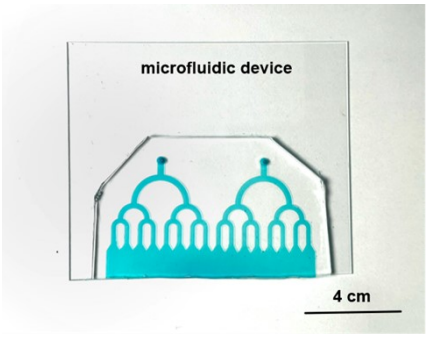

Fig. S2 Optical photographs of the prepared microfluidic device.

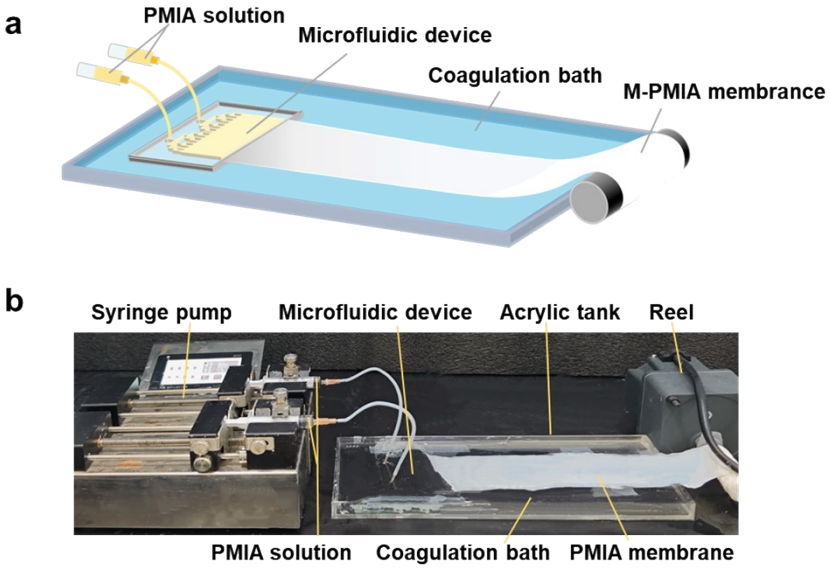

Fig. S3 (a) Schematic and (b) photographic images of PMIA membrane fabrication via microfluidic technology.

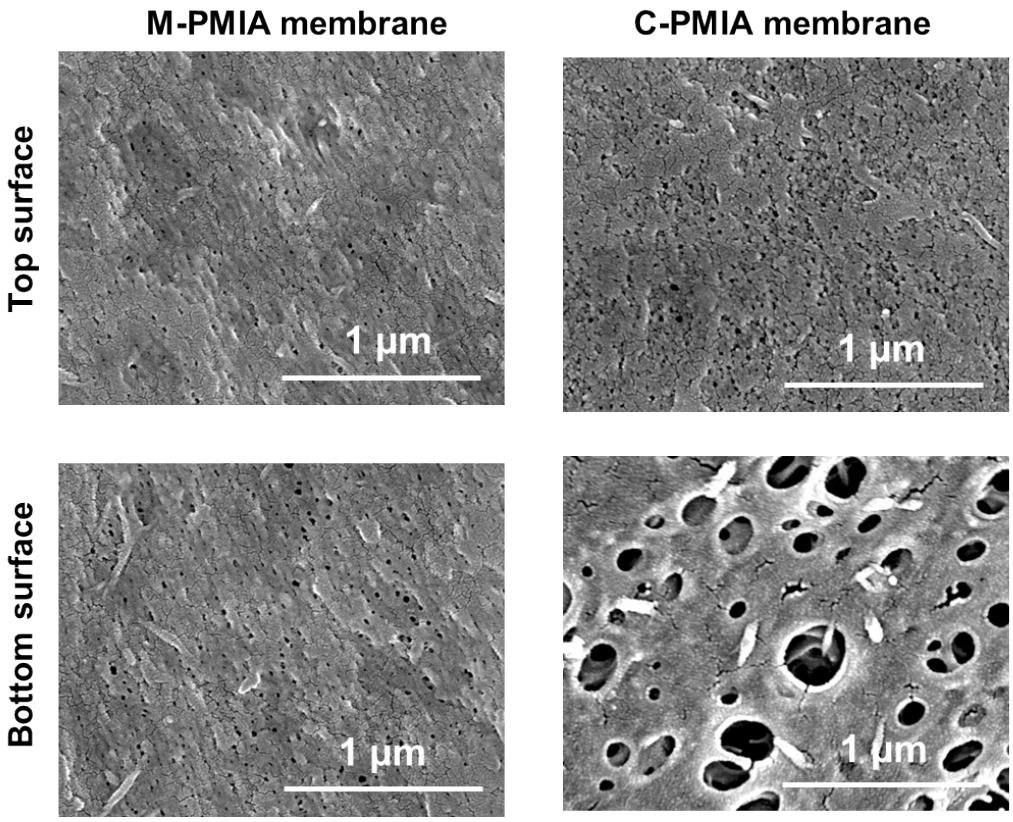

Fig. S4 Top and bottom surface SEM images of the M-PMIA and C-PMIA membranes.

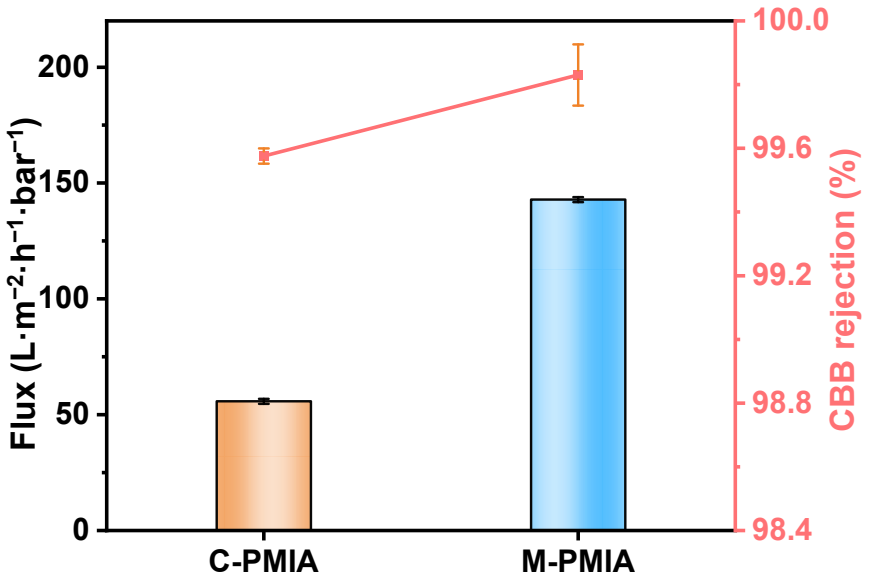

Fig. S5 CBB dye solution separation performance of the M-PMIA and C-PMIA membranes.

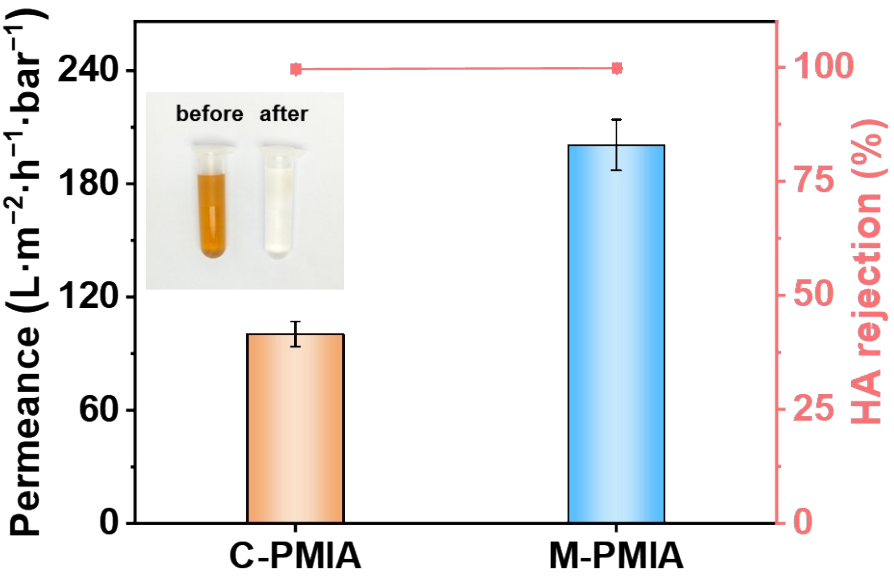

Fig. S6 Separation performance of M-PMIA and C-PMIA membranes for HA.

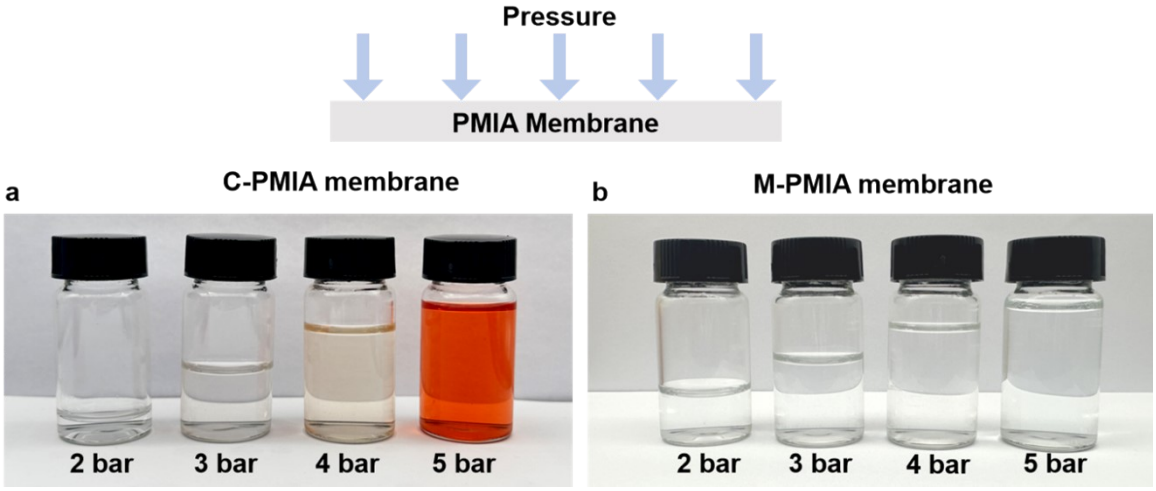

Fig. S7 Optical photograph of CR dye solution after (a) C-PMIA and (b) M-PMIA membrane separation under different pressure conditions.

Fig. S8 Images of water contact angles of the M-PMIA and C-PMIA membranes.

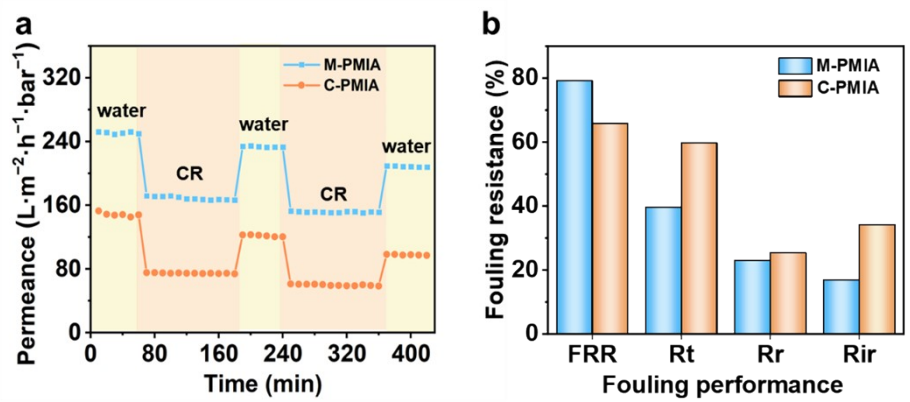

Fig. S9 (a) Anti-fouling performance of the M-PMIA and C-PMIA membranes (b) The corresponding anti-fouling indexes (*FRR*, R_t, R_r, R_{ir}) of the M-PMIA and C-PMIA membranes.

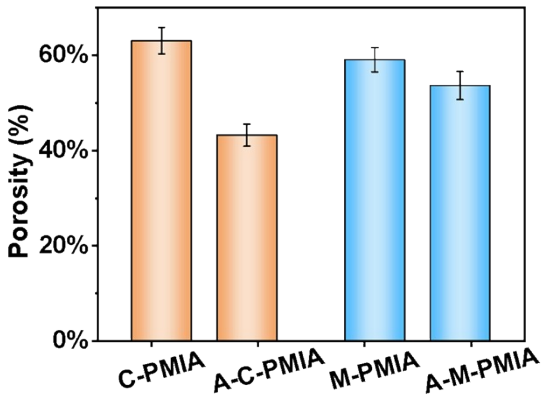

Fig. S10 Porosity of the C-PMIA membranes and M-PMIA membranes before and after 1.5 hours testing under 2 bar pressure of pure water.

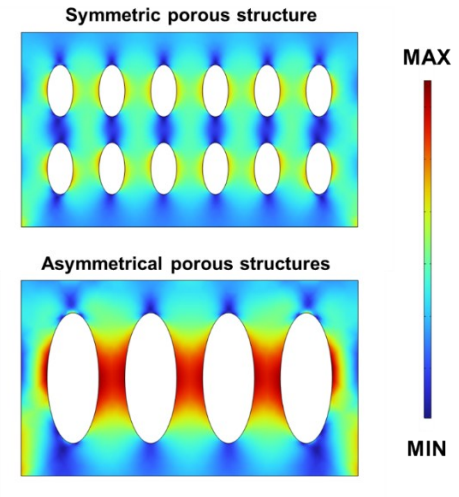

Fig. S11 Finite element simulation of stress distribution in symmetric and asymmetric pore structures.

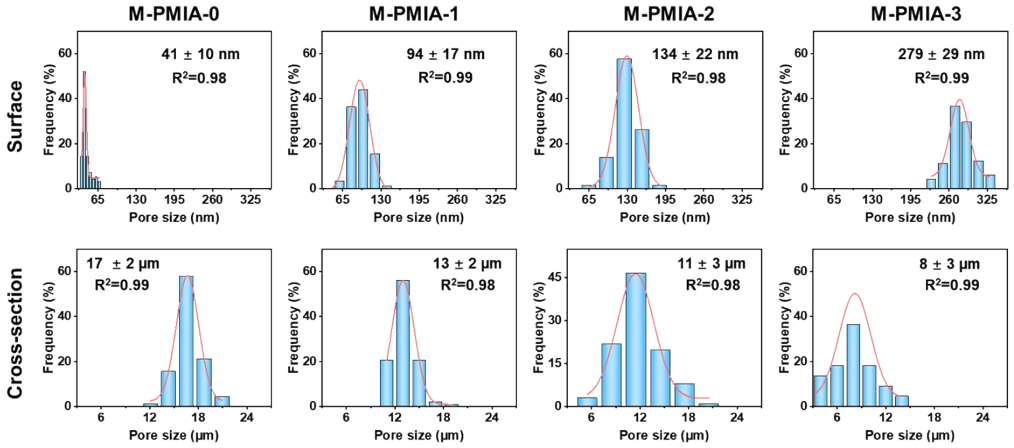

Fig. S12 The pore size distribution curves of surface and cross-sectional pores.

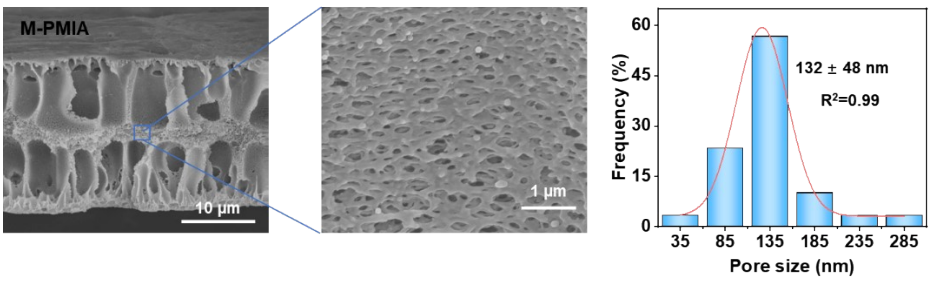

Fig. S13 The pore size distribution curve of the magnified cross-sectional spongy pore region.

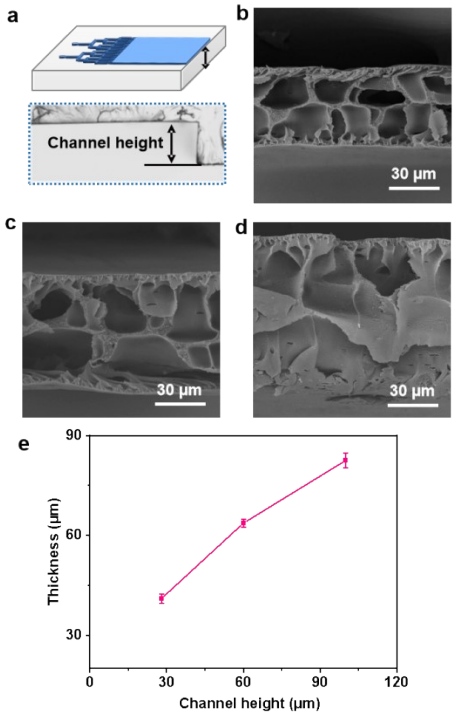

Fig. S14 Regulation of the thickness of the M-PMIA membranes. Thickness of the M-PMIA membranes by varying the microfluidic channel heights. (a) Optical photographs of the microchannel. (b) (c) and (d) SEM images of the M-PMIA membranes with different thicknesses. (e) The correlation between the thickness of the M-PMIA membranes and the microchannel heights.

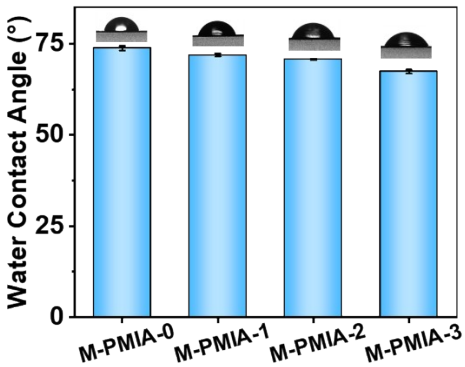

Fig. S15 Water contact angle of the M-PMIA membranes.

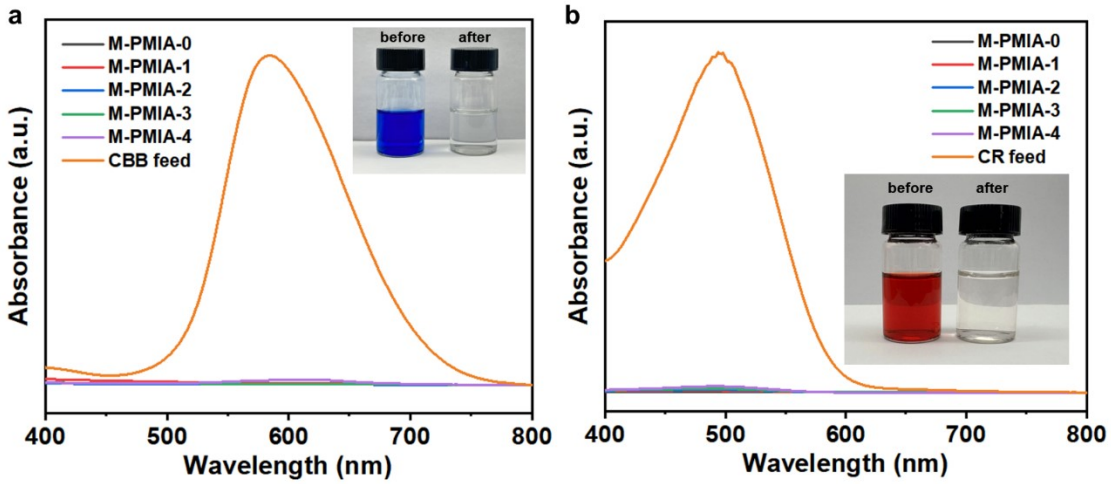

Fig. S16 UV–vis spectra of (a) CBB dye and (b) CR dye solutions before and after separation by the M-PMIA membranes.

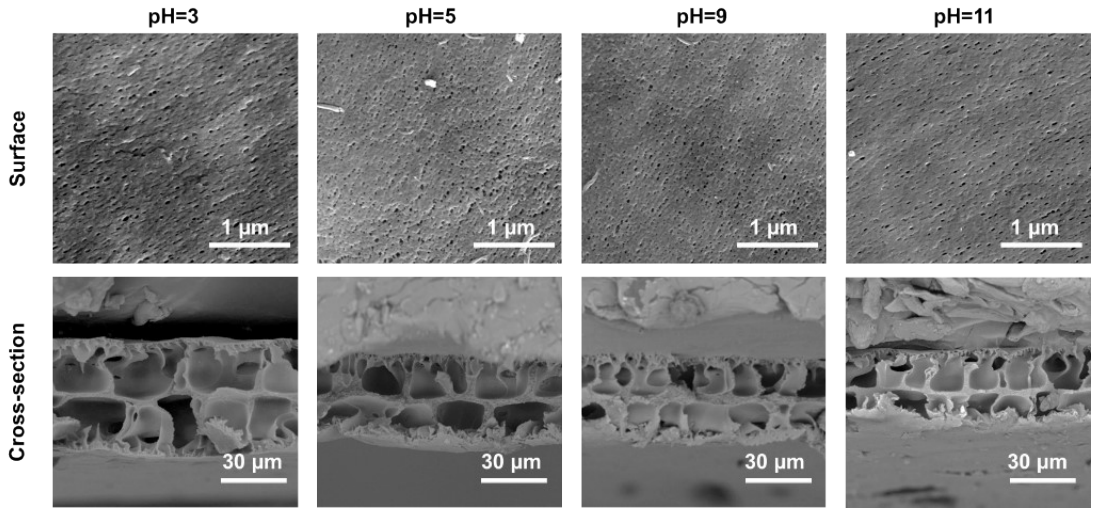

Fig. S17 Surface and cross-sectional SEM images of the M-PMIA-1 membrane after 72 h of immersion in solutions with different pH.

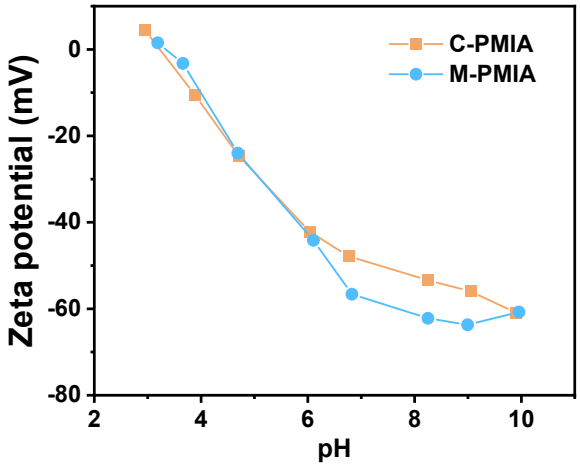

Fig. S18 Surface potential of the C-PMIA and M-PMIA membranes.

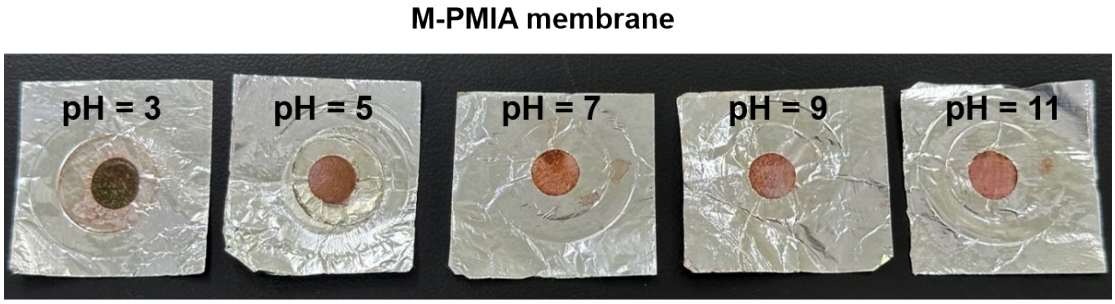

Fig. S19 Optical photograph of M-PMIA membrane after testing in different pH dye environments.

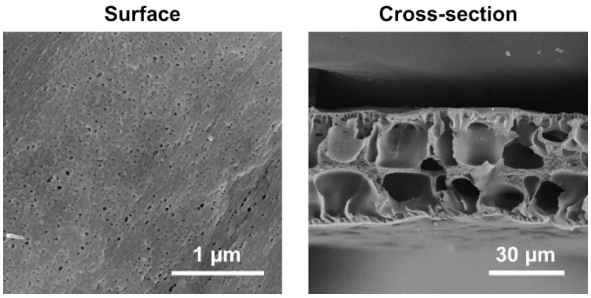

Fig. S20 Surface and cross-sectional SEM images of the M-PMIA-1 membrane after heating at 70℃ for 72 h.

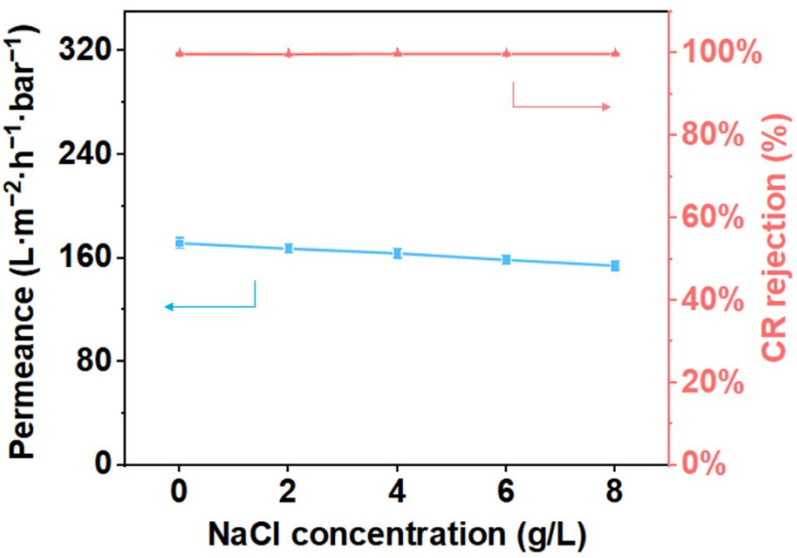

Fig. S21 Separation performance of the M-PMIA-1 membrane in 100 ppm Congo red mixed with NaCl solutions at different concentrations.

Table S1 Performance comparison of the M-PMIA membranes and reported TUF membranes.

Membrane type	CR Permeability ($L \cdot m^{-2} \cdot h^{-1} \cdot bar^{-1}$)	CR rejection	Operating condition (MPa)	Structure feature	Stress (MPa)	Breaking elongation	Young's modulus (MPa)	References
PES/PAES	23	96%	0.6	Finger-like pore structure	6	50%	—	[1]
AMPS-PANI	95	98.8%	0.1	Finger-like pore structure	12.6	42.5%	75.4	[2]
TOCNF-PEI-GA	27	99.75%	0.3	Finger-like pore structure	18.7	22.38%	243.1	[3]
PES/SPSF	76	99.2%	0.1	Sponge-like pore structure	6.9	—	—	[4]
PI/SiO_2	133	91.21%	0.4	Finger-like pore structure	2.6	—	—	[5]
SPAA6/S20	6	99.8%	0.1	Sponge-like pore	2.9	—	—	[6]
PI/AA-CMMT	95	98%	0.3	Finger-like pore structure	—	—	—	[7]
PES-SPSF/PD	61	99.7%	0.1	Finger-like pore structure	—	—	—	[8]
Polyester	88	99.2%	0.1	Finger-like pore structure	—	—	—	[9]
M-PMIA	180	99.8%	0.2	Symmetric porous structure	4.3	18%	59.3	This work

References

1. H. Cui, S. Fan, Z. Zhou, Y. Du, W. Chen, C. Xiang, J. Zhang, D. Wang, S. Zhang, P. Zhang and H. Matsuyama, *Sep. Purif. Technol.*, 2025, **376**, 133935.
2. S. Liu, H. Jiang and Y. Li, *Chem. Eng. J.*, 2023, **467**, 143456.
3. L. Du, C. Li, S. Li, W. Zhang and F. Huang, *Chem. Eng. J.*, 2025, **521**, 166706.
4. M. Hu, Z. Cui, S. Yang, J. Li, W. Shi, W. Zhang, C. Matindi, B. He, K. Fang and J. Li, *J. Membr. Sci.*, 2021, **618**, 118746.
5. Z. Liu, R. Qiang, L. Lin, X. Deng, X. Yang, K. Zhao, J. Yang, X. Li, W. Ma and M. Xu, *J. Membr. Sci.*, 2022, **658**, 120747.
6. D. Liu, Z. Zhu, Y. Zhao, Y. Chen, Y. Tan and Y. Zhang, *Science of The Total Environment*, 2019, **695**, 133908.
7. W. Ma, X. Yang, L. Lin, H. Li, H. Shang, H. Wu, M. Hou, Z. Guo, Z. Liu, J. Yang and B. Li, *J. Membr. Sci.*, 2025, **723**, 123937.
8. Y. Zhao, Y. Liao, G. S. Lai, Y. Yin and R. Wang, *J. Membr. Sci.*, 2023, **685**, 121908.
9. M.-M. Tang, X.-G. Jin, X. Tang, M. Yu, X.-H. Ma and Z.-L. Xu, *Sep. Purif. Technol.*, 2025, **353**, 128476.